

Biharmonic pattern selection

Wei Wang

*Condensed Matter Group, International Centre for Theoretical Physics, P.O. Box 586, 34100 Trieste, Italy
and Physics Department, The Centre for Nonlinear Dynamical Systems,
Nanjing University, Nanjing, People's Republic of China*

E. Canessa

Condensed Matter Group, International Centre for Theoretical Physics, P.O. Box 586, 34100 Trieste, Italy
(Received 17 August 1992; revised manuscript received 16 September 1992)

A model to describe fractal growth is introduced that includes effects due to long-range coupling between displacements u . The model is based on the biharmonic equation $\nabla^4 u = 0$ in two-dimensional isotropic defect-free media as follows from the Kuramoto-Sivashinsky equation for pattern formation—or, alternatively, from the theory of elasticity. As a difference with Laplacian and Poisson growth models, in this model the Laplacian of u is neither zero nor proportional to u . Its discretization allows one to reproduce a transition from dense to multibranching growth at a point in which the growth velocity exhibits a minimum similarly to what occurs within Poisson growth in planar geometry. Furthermore, in circular geometry the transition point is estimated for the simplest case from the relation $r_\ell \approx L/e^{1/2}$ such that the trajectories become stable at the growing surfaces in a continuous limit. Hence, within the biharmonic growth model, this transition depends only on the system size L and occurs approximately at a distance 60% far from a central seed particle. The influence of biharmonic patterns on the growth probability for each lattice site is also analyzed.

PACS number(s): 68.70.+w, 61.50.Cj, 05.40.+j, 03.40.Dz

I. INTRODUCTION

The study of pattern formation in physically important fields by using simple lattice models under certain boundary conditions is of great interest because the fields describe many phenomena that occur in nature. At present, numerical simulation studies include, e.g., the dielectric breakdown model (DBM), i.e., solving the Laplacian equation in the medium surrounding the growing aggregates [1–3], and the Poisson growth model of the pattern formation in screened electrostatic fields [4]. Besides, the diffusion-limited aggregation (DLA) model also plays a crucial role in illustrating fractal growth [5–7]. So far, much effort has been invested in such stochastic models that share the common feature of being essentially second-order differential equations. In these models iterative procedures are carried out around *four* mesh points of a lattice to then phenomenologically relate the global influence of a growing pattern to the growth probability for each lattice site under different power-law forms (see, e.g., [8]).

Nevertheless, there is also another important class of physical problems leading to partial differential equations that can also be linear in the order parameter but, as a peculiarity, they are of higher order and directly concern the issue of pattern formation. An example of this is the (time-averaged) Kuramoto-Sivashinsky equation [9, 10]:

$$\frac{\partial u}{\partial t} = \nu \nabla^2 u + \lambda \nabla^2 \nabla^2 u + \mu (\nabla u)^2, \quad (1)$$

which models pattern formation in different physical contexts, such as chemical reaction-diffusion systems [11, 12] and a cellular gas flame in the presence of external stabilizing factors [13]. In the above ν , λ , and μ are normalized coefficients and u a displacement at time t .

If we consider the simplest case, i.e., assume static solutions and keep linear terms only (i.e., $\mu \equiv 0$), then Eq. (1) reduces to the sum of two important terms: the Laplacian equation plus the biharmonic equation

$$\nabla^4 u = \nabla^2 (\nabla^2 u) = 0. \quad (2)$$

Since the former term (i.e., $\lambda = 0$), when discretized, is known to display fractal structures on a squared lattice [1, 2], then the latter term [i.e., Eq. (2)] might also in fact select a new class of fractal patterns.

In addition to the above physical relevance, the biharmonic part of Eq. (1) can describe the deflection of a thin plate subjected to uniform loading over its surface with fixed edges [3, 14], the steady slow two-dimensional (2D) motion of a viscous fluid [15], or the vibration modes in the acoustics of drums [16]. Besides this a higher-order differential equation containing the biharmonic term also appears in the study of kinetic growth with surface relaxation (see, e.g., [17–20]).

As an important difference with respect to second order, solving numerically higher-order differential equations, such as the one at hand, requires values for the order parameters at either their first or second normal

derivatives at each boundary point and beyond [21, 22]. Hence, an analysis of effects due to long-range (many-body) coupling of lattice sites, including those mesh points at the lattice boundaries, on the formation of connected patterns, is by no means trivial and as such it is a completely open problem. This is the subject of this paper.

In the following we shall discuss an attempt to include higher nearest-neighbor (displacements) shells in numerical simulations of fractal growth in isotropic defect-free media of arbitrary elastic constants. We achieve this by (analytically and numerically) studying Eq. (2) under the condition that the Laplacian of u is not constant (i.e., Laplace's case) or proportional to u (i.e., Poisson's case) along a growing surface. Since this biharmonic operator can also be generated in the theory of elasticity [14, 23, 24], then $\mathbf{u} \equiv \mathbf{r} - \mathbf{r}'$ may become the displacement vector and the deformation of a body may be caused by an *applied* force which appears in the solution of Eq. (2) through some boundary conditions [Eq. (4) below].

$$u_{i-2,j} + 2u_{i-1,j-1} - 8u_{i-1,j} + 2u_{i-1,j+1}$$

$$+ u_{i,j-2} - 8u_{i,j-1} + 20u_{i,j} - 8u_{i,j+1} + u_{i,j+2} + 2u_{i+1,j-1} - 8u_{i+1,j} + 2u_{i+1,j+1} + u_{i+2,j} = 0. \quad (3)$$

It is important to mention that numerical simulations using this equation are somehow more involved than for Laplace [1] or Poisson [4] growth because of long-range coupling. However, the accuracy of the solution for Eq. (3) can similarly be improved by looking at the convergence of the iterative solution using the Gauss-Seidel method [21].

Equation (2) requires modification when applied at mesh points that are adjacent to a boundary, since one (at the edge) or two (near the corners) of the values needed are at sites outside the lattice. This modification is made by introducing a fictitious mesh point at (i, L) outside the planar lattice in the y direction, where the value of u is given there by the derivative boundary condition along one edge boundary:

$$u_{i,L+1} = u_{i,L-1} + 2h \left. \frac{\partial u}{\partial y} \right|_{i,L}. \quad (4)$$

Here h ($= h_x = h_y$) is the mesh size which we set equal to unity for simplicity. For planar geometry, we evaluate Eq. (4) approximating

$$\left. \frac{\partial u}{\partial y} \right|_{i,L} \approx \frac{3(u^o - u^i)}{L}, \quad (5)$$

for all i columns. This expression is obtained after taking the limit $\ell/L \ll 1$ in the solution of a one-dimensional biharmonic equation. Also for simplicity, the values of $u(i, 0)$ for the points below the seed will be set to zero. For circular geometry we treat the boundary conditions similarly to Laplacian growth [1], i.e., all the lattice sites outside a circle of radius r are set equal to u^o , hence, we

II. NUMERICAL SIMULATION

In this work, the numerical simulation of Eq. (2) is carried out on a lattice with either planar (i.e., growth in a channel) or circular (i.e., radial growth) geometries. Within the planar geometry we use a 100×200 lattice, having periodic boundary conditions along the x direction, and set the values $u^o = 1$ and $u^i = 0$ for the upper y boundary and the surface aggregate ($y = \ell$), respectively. Initially, seed particles are placed on a line at displacement $u(i, 1)$. For circular geometry, we use lattice sites enclosed within a circumference of radius $r = 100$ and locate only one seed at the center such that u^o and u^i are also unity and zero at the outer (circular) boundary and at the inner (growing) aggregate, respectively.

The inclusion of (second and higher) nearest-neighbor bond shells in our numerical simulations follows the discrete form of Eq. (2) on the (i, j) lattice site, which yields an expression involving values of u at 13 mesh points written as [21]

approximate for the sake of simplicity $\partial u / \partial y|_{y=L} \approx 0$ in the absence of applied field.

The procedure for growing our biharmonic aggregates follows standard techniques [1]. First, Eq. (2) is solved iteratively until the solutions converge to a given accuracy (of the order 3×10^{-3} or smaller). Second, after adopting a growth probability law, the aggregates stochastically grow at one (or more) perimeter(s) under a given relation between u and growth probability P .

In order to have biharmonic pattern selection we shall assume that P at the grid site (i, j) depends on two different phenomenological (normalized) forms, namely

$$P_{ij} = \begin{cases} \frac{|\nabla^2 u_{i,j}|}{\sum |\nabla^2 u_{ij}|} & \text{(model I)} \\ \frac{|u_{i,j}|}{\sum |u_{ij}|} & \text{(model II)} \end{cases},$$

where the sum runs over all of the nearest-neighbor sites to an aggregate. Model I implies that P_{ij} is proportional to the local potential, similarly to DBM [1, 4, 8], whereas in model II, P_{ij} is proportional to displacements around the (i, j) site.

III. RESULTS AND DISCUSSION

As already mentioned we attempt to study the effects of long-range coupling of displacements in simulations of fractal growth. To achieve this, we start analyzing the numerical solutions of Eq. (2) in planar geometry. In Figs. 1(a), 1(b), and 1(c) we show three characteristic stages of growing for a biharmonic pattern by attaching one particle at each step and assuming model I for the probability P_{ij} . Figure 1(a) includes 2100 parti-

cles, 1(b) 4164 particles, and 1(c) 4355 particles added to the biharmonic cluster. In these numerical simulations we estimate the derivative boundary condition [cf., Eq.(4)] from the analytical solution given by Eq. (5) and fix $u^i = 0$ and (rescaled) $\phi^o \equiv \nabla^2 u|_{y=L} \approx 6u^o/L^2$ such that $u^o = 1$. Clearly, at a distance separation of about $\ell \sim 160$, Fig. 1(c) displays features of a transition from dense to multibranched growth similarly to what occurs within Poisson growth in planar geometry [4]. This struc-

ture demonstrates that long-range coupling of displacements drives such phenomena.

Surprisingly, such a transition also appears when we consider model II for P_{ij} as can be seen in Fig. 2 for a biharmonic cluster containing 3428 particles. This means that the influence of ramified biharmonic patterns on the growth probability for each lattice site is on the type of the (far from equilibrium) pattern obtained and not on locating the transition. We add that several branches

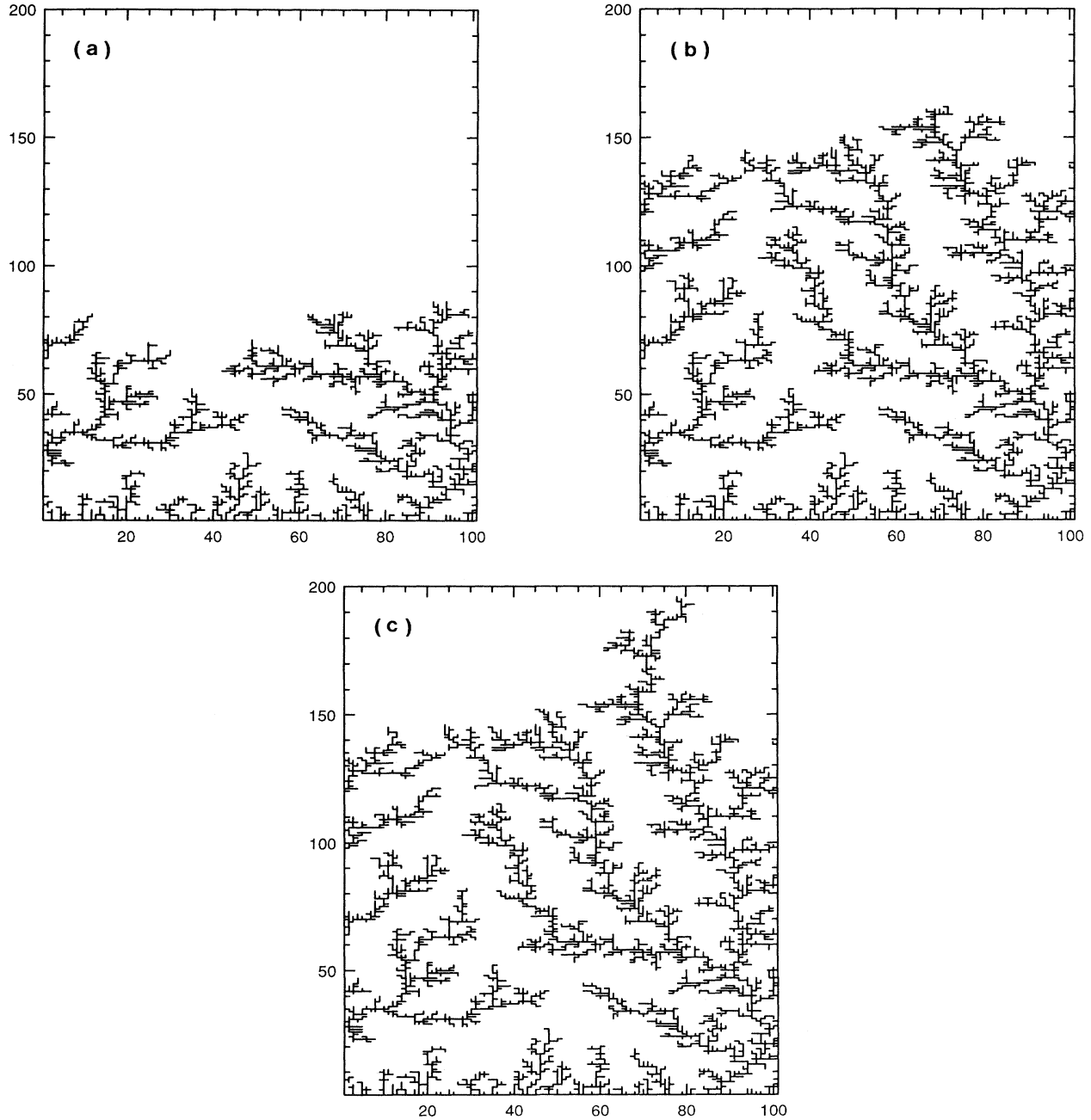


FIG. 1. Three characteristic stages of growing for a biharmonic pattern by attaching one particle at each step and assuming model I for the probability P_{ij} : (a) 2100, (b) 4164, and (c) 4355 added particles to display the transition from dense to multibranched growth.

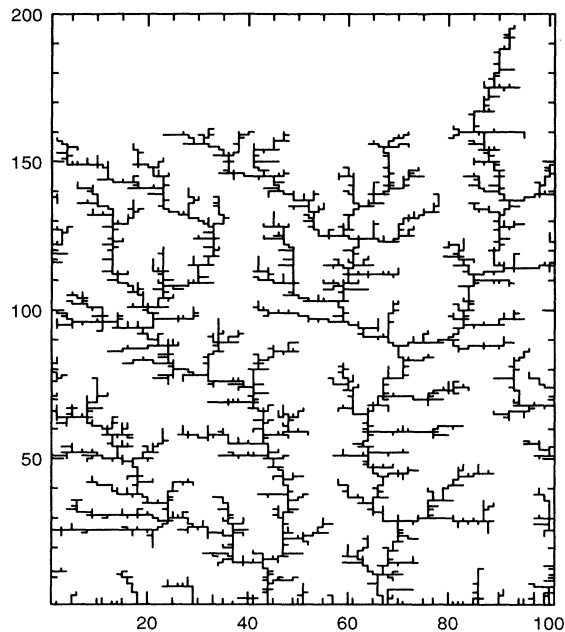


FIG. 2. Final biharmonic pattern above the transition when considering model II for P_{ij} and 3428 particles.

may also develop within our biharmonic growth model by attaching, simultaneously and stochastically, more than one particle at each time step similarly to the work of Louis *et al.* [4]. We believe that for Poisson growth this transition is the result of including many-body contributions via screening in a sort of mean-field approach. In our biharmonic model, long-range coupling appears naturally as a consequence of dealing with Eq. (2). As we shall show next for the case of planar growth, the transition point within both Poisson and biharmonic models appears when the growth velocities exhibit a minimum.

In Fig. 3 we plot results for the growth velocity v along the y direction for biharmonic growth under model I (curve A), i.e., proportional to the averaged value of P equal to $\nabla^2 u$ to consider explicitly nearest-neighbor sites, and under model II (curve B), where it has been set proportional to the local displacement u . For comparison, we also include in this figure results for Poisson growth, i.e., $\nabla^2 \phi = \mu \phi$ [4], such that v is set proportional to the field $|\phi_{i,j} - \phi^i|$ following Ref. [4]. The Poisson growth model incorporates screening (curve C), i.e., $\mu = \lambda^2$, and antiscreeing (curve D), i.e., $\mu = -\lambda^2$.

In this plot it can be seen that the transition from dense to multibranch growth coincides with the fact that v on the growing surface presents a minimum. This was pointed out by Louis *et al.* [4] for the case of screening (curve C) (which also applies for antiscreeing as seen in curve D). However, from the present findings, we can argue that this is also true for biharmonic growth (curves A and B) independently of how we have related the probability P_{ij} to $u(i, j)$. For Laplacian growth this phenomenon does not appear since the trend is to generate a single tip at faster velocity than in the cases of Poisson or biharmonic growth. It is worthwhile to point out

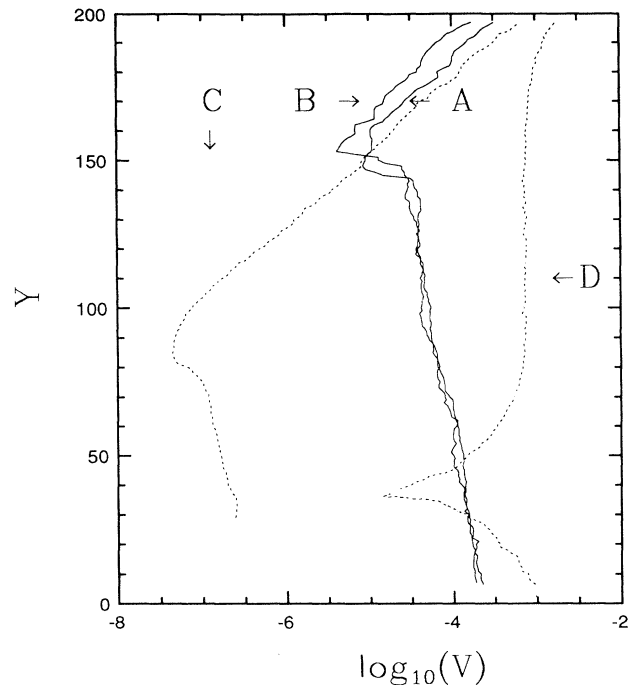


FIG. 3. Growth velocity v along the y direction proportional to $|\nabla^2 u|$ (curve A) and displacement $|u|$ (curve B). Curves C and D are for Poisson growth including screening and antiscreeing, respectively.

that biharmonic patterns below the transition point, i.e., within the dense region (see Figs. 1 and 2), become not as dense as for screening [4], but are rather denser than for antiscreeing (not shown). Indeed, this can easily be understood from Fig. 3 since for Poisson growth (screening), such that $\mu > 0$, the transition occurs at smaller velocities than for biharmonic growth. Henceforth, an Eden-like pattern can be generated due to screening [4]. Above the transition multibranch fractals appear in all models considered, but within our biharmonic model the transition point depends on the system size only (as it will become clear below). We remark that both Poisson and biharmonic models lead to obtaining growth velocities along the y direction with parallel slopes above and below their respective transition points. We feel this to be a particular feature of fractal growth due to long-range coupling of displacements.

Let us focus next on effects due to long-range coupling on the fractal growth in circular geometry. This will allow us to make calculations of the fractal dimension for the biharmonic patterns by the standard box counting method [3]. To generate and select biharmonic fractal structures we set, for simplicity, the derivative boundary condition required along the r direction equal to zero. Figures 4(a) and 4(b) show the results for circular biharmonic growth using again models I (where P is set proportional to $\nabla^2 u$, which corresponds to the potential in [4]) and II, respectively. Figure 4(a) includes 2326 particles whereas Fig. 4(b) has 2172 particles. It can immediately be seen that above a certain transition point,

say r_ℓ , these plots give another demonstration that long-range coupling is the most relevant aspect for the transition independently of the geometry adopted or of the given relation between P_{ij} and $u(i, j)$.

The transition point r_ℓ can, to a good approximation, be estimated from the continuous limit of Eq.(2) in cylindrical coordinates, such that $z = 0$ for all polar angles θ , namely,

$$\frac{1}{r^2} \left(\frac{\partial u}{\partial r} \right) - \frac{1}{r} \left(\frac{\partial^2 u}{\partial r^2} \right) + 2 \left(\frac{\partial^3 u}{\partial r^3} \right) + r \left(\frac{\partial^4 u}{\partial r^4} \right) = 0 \quad , \quad (6)$$

whose solution (far from the origin) is

$$u = A + Br^2 + C \ln r + Dr^2 \ln r \quad . \quad (7)$$

Clearly, two of the four coefficients A , B , C and D may

be determined by the boundary conditions of the problem, i.e., by assuming that at $r = r_\ell$, $u(r_\ell) = u^i \equiv 0$, whereas at $r = L$, $u(L) = u^o \equiv 1$. However, as discussed above, in addition to this we also have the condition required by simulations [cf., Eq. (4)]: $\partial u / \partial r |_{r=L} \equiv 0$, which leads to the following relation between B , C , and D :

$$\frac{B}{D} = - \frac{C/D}{2L^2} - (\ln L + \frac{1}{2}) \quad . \quad (8)$$

This, in conjunction with one possible condition of stability for the trajectories at the growing surfaces, which is obtained from $\partial u / \partial r |_{r=r_\ell} \sim 0$, i.e., $B/D = -(\ln r_\ell + 1)$ and $C = 0$, gives

$$r_\ell \approx \frac{L}{e^{1/2}} = 0.607L. \quad (9)$$

Hence, we have that the transition point only depends on the system size L and occurs approximately at a distance (in lattice units) about 60% far from the seed particle as indicated by arrows in Figs. 4(a) and 4(b). Nicely, our simplest prediction is in accord with the numerical simulations. But if the derivative boundary condition $\partial u / \partial r |_{r=L}$ is a constant different from zero, then Eq. (8) changes by a factor which, together with the above stability conditions, implies a shift of the transition length and a more complicated relation between r_ℓ and L .

To end this section, we examine the fractal properties of the simulated biharmonic patterns displayed in Figs. 4(a) and 4(b), by simply counting the number of particles $N(r)$ inside a circle of increasing radius r (in lattice units) around a seed particle at the origin until we reach a distance r_ℓ at which the transition appears [cf., Eq. (9)]. We then plot it as a function of r in a log-

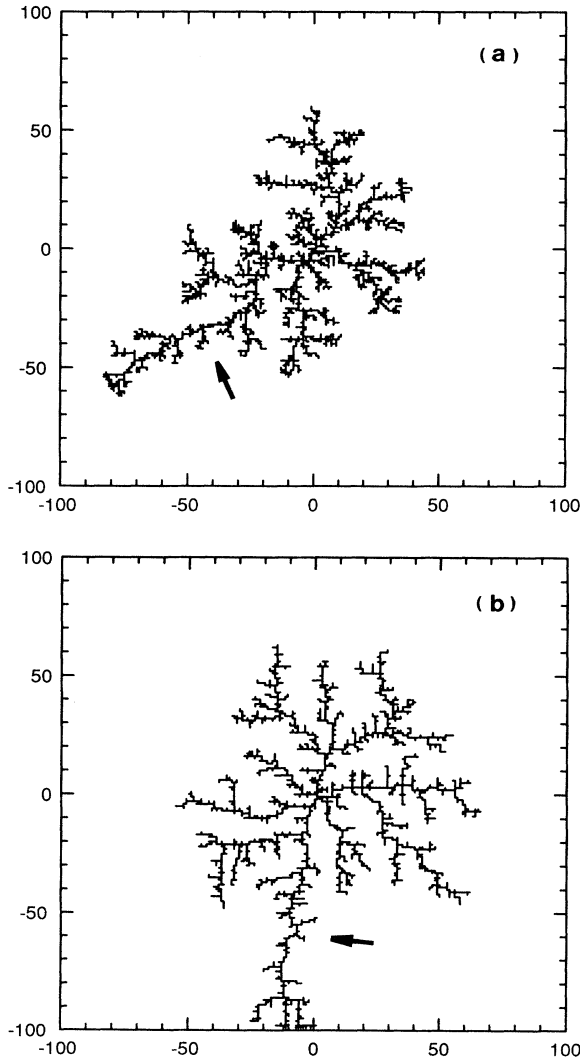


FIG. 4. Results for circular biharmonic growth using (a) model I with 2326 particles and (b) model II with 2172 particles. Arrows indicate predicted transition points from Eq. (9).

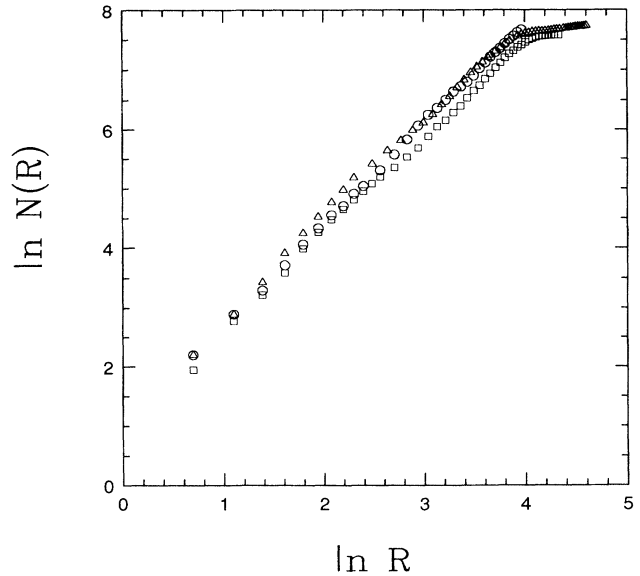


FIG. 5. Fractal nature of the simulated biharmonic patterns that are displayed in Figs. 4(a) and 4(b). Triangles are obtained using model I and squares using model II. Circles are for Laplacian growth giving a fractal dimension of ~ 1.7 .

log plot, as depicted in Fig. 5, for models I (triangles) and II (squares) which we compare to Laplacian growth (circles). Over a decade, we obtain lines with slopes larger than unity and smaller than the space dimension. Thus, to a first approximation, the fractal dimension of our biharmonic patterns in the denser region approaches the value due to DBM (and DLA) within error bars [1]. This illustrates the fractal nature of the biharmonic patterns. Above r_ℓ , there is a change of slope due to the transition from dense to multibranching growth contrary to the curve from the Laplacian model (circles) which continues to be linear, indicating thus that the cluster grows dense.

IV. CONCLUDING REMARKS

In this work, we have shown that the discretization of the biharmonic Eq. (2) allows us to reproduce a transition from dense to multibranching growth at a point in which the growth velocity v along the y direction exhibits a minimum similarly to what occurs within Poisson growth in planar geometry. The physical basis for v , as plotted in Fig. 3, follows similarly to the dielectric breakdown model (model I: curve A), namely, assuming v to be proportional to the averaged value of P equal to the potential $\nabla^2 u$, to thus consider explicitly nearest-neighbor sites; model II, curve B , where v has been set proportional to the local displacement u , is simply a mathematical model. On the other hand, we also discussed that in circular geometry the transition point can be estimated from the relation $r_\ell \approx L/e^{1/2}$ such that the trajectories become stable at the growing surfaces in a continuous limit. This is in reasonable agreement with present numerical simulations. Hence, we conclude that the transition from dense to multibranching growth

within a biharmonic approach depends on the system size L only.

The transition obtained from numerically solving the biharmonic equation might not be necessarily similar to the intriguing Hecker transition (see, e.g., [25, 26]). But, to this end, we notice that when assuming in the Kuramoto-Sivashinsky relation (1) $\nu < 0$ and $\lambda > 0$, then we obtain (see also [9])

$$\frac{\partial \mathbf{v}}{\partial t} = -\nabla^2 \mathbf{v} + \nabla^2 \nabla^2 \mathbf{v} + 2\mathbf{v} \cdot \nabla \mathbf{v} \quad , \quad (10)$$

in which $\mathbf{v} = \nabla u$ and $\text{curl } \mathbf{v} = 0$. This looks somewhat like the Navier-Stokes equation (for a potential flow with negative viscosity) which may be somehow related to the recent analysis in Ref. [26] of electrochemical deposition.

Finally, it is important to emphasize again that, as a crucial difference to those models satisfying second-order differential equations, to select fractal structures via the biharmonic part of Eq. (1) requires values for the order parameters (at either their first or second normal derivatives at each boundary point) and the (second and higher) nearest-neighbor bond shells on the (i, j) lattice site which yields an expression involving values of u at 13 mesh points. Thus, the formation of connected patterns within the biharmonic equation is not trivial at all. Because of this, our numerical simulations are more involved than for Laplace (or Poisson) fractal growth due to the *long-range coupling* between displacements.

ACKNOWLEDGMENTS

The authors would like to thank the Condensed Matter Group, the Computer Section, and Professor Abdus Salam at ICTP, Trieste, for support.

-
- [1] L. Niemeyer, L. Pietronero, and H.J. Wiesmann, Phys. Rev. Lett. **52**, 1033 (1984).
 - [2] E. Arian, P. Alstrøm, A. Aharony, and H.E. Stanley, Phys. Rev. Lett. **63**, 2005 (1989).
 - [3] E. Canessa and B. Tanatar, Phys. Rev. A **44**, 3471 (1991).
 - [4] E. Louis, F. Guinea, O. Pla, and L.M. Sander, Phys. Rev. Lett. **68**, 209 (1992).
 - [5] H. La Roche, J. F. Fernández, M. Octavio, A.G. Loeser, and C.J. Lobb, Phys. Rev. A **44**, R6185 (1991).
 - [6] R.W. Bowel and S.D. Collins, Phys. Rev. A **43**, 3165 (1991).
 - [7] A. Arneodo, F. Argoul, E. Bacry, J.F. Muzy, and M. Tabard, Phys. Rev. Lett. **68**, 3456 (1992).
 - [8] P. Meakin, J. Feder, and T. Jøssang, Phys. Rev. A. **43**, 1952 (1991).
 - [9] Y. Kuramoto, Suppl. Prog. Theor. Phys. **64**, 346 (1978).
 - [10] G.I. Sivashinsky, Acta Astron. **6**, 569 (1979).
 - [11] J.M. Hyman and B. Nicolaenko, Physica D **18**, 113 (1986).
 - [12] B.I. Shraiman, Phys. Rev. Lett. **57**, 325 (1986).
 - [13] B.A. Malomed and M.I. Tribelsky, Physica D **14**, 67 (1984).
 - [14] L.D. Landau and E.M. Lifshitz, *Theory of Elasticity* (Pergamon, New York, 1959).
 - [15] H. Lamb, *Hydrodynamics*, 6th ed. (Cambridge University Press, London, 1932).
 - [16] T. Rossing, Phys. Today **45**, 40 (1992).
 - [17] D.E. Wolf and J. Villain, Europhys. Lett. **13**, 389 (1990).
 - [18] Z.-W. Lai and S. Das Sarma, Phys. Rev. Lett. **66**, 2348 (1991).
 - [19] P.-M. Lam and F. Family, Phys. Rev. A **44**, 4854 (1991).
 - [20] H. Yan, Phys. Rev. Lett. **68**, 3048 (1992).
 - [21] G. de Vahl Davis, *Numerical Methods in Engineering and Science* (Allen & Unwin, London, 1986).
 - [22] J.C. Buell, J. Comp. Phys. **95**, 313 (1991).
 - [23] R.C. Ball and R. Blumenfeld, Phys. Rev. Lett **65**, 1784 (1990).
 - [24] P. Meakin, G. Li, L.M. Sander, E. Louis, and F. Guinea, J. Phys. A **22**, 1393 (1989).
 - [25] V. Fleury, M. Rosso, J.-N. Chazalviel and B. Sapoval, Phys. Rev. A **44**, 6693 (1991).
 - [26] V. Fleury, J.-N. Chazalviel, and M. Rosso, Phys. Rev. Lett. **68**, 2492 (1992).